# ASSESSING IMPACTS OF GRASS ON VERTICAL ACCURACY OF DIGITAL SURFACE MODELS DERIVED FROM UNMANNED AIRCRAFT SYSTEMS IMAGERY

By

AMANDA F. THOMAS

Bachelor of Science in Agriculture

Oklahoma State University

Stillwater, Oklahoma

2016

Submitted to the Faculty of the
Graduate College of the
Oklahoma State University
in partial fulfillment of
the requirements for
the Degree of
MASTER OF SCIENCE
December, 2018

ASSESSING IMPACTS OF GRASS ON VERTICAL ACCURACY

OF DIGITAL SURFACE MODELS DERIVED FROM

UNMANNED AIRCRAFT SYSTEMS IMAGERY

Thesis Approved:

Dr. Amy E. Frazier

Thesis Adviser

Dr. Carlos Cordova

Committee Chair

Dr. Adam J. Mathews

# ACKNOWLEDGEMENTS

I would like to give my thanks appreciation to everyone who made my research successful and assisted me at every point to cherish my goal, and attain this degree.

First, my sincere thanks to my thesis advisor Amy Frazier. My research would not have been possible without the aid of her unyielding motivation, patience, and ideas. Thanks also to Adam Mathews for coordinating the collection of the data used in this project, for providing guidance, and encouraging my research. It is whole-heartedly expressed that Amy and Adam's advice proved to be a landmark effort towards the success of this project.

My sincere thanks go to Carlos Cordova for serving on my committee, and for his knowledge and encouragement.

I would also like to thank Oklahoma Department of Recreation and Tourism for their support, and funding.

I am profoundly grateful to Catherine Shropshire for assisting in data collection, her unwavering support, and for riding this train with me.

Finally, I must express special thanks to my parents Teri and Allen, my sister Jackie, Grandma JoNell, and especially to my husband Patrick for providing me with unfailing support, love, and continuous encouragement throughout my years of study and through the process of researching and writing this thesis.

Thank you all,

Amanda F. Thomas (Lind)

Name: Amanda F. Thomas

Date of Degree: DECEMBER, 2018

Title of Study: ASSESSING IMPACTS OF GRASS ON VERTICAL ACCURACY OF DIGITAL SURFACE MODELS DERIVED FROM UAS

Major Field: GEOGRAPHY

Abstract: Digital surface models (DSM), which are 3D representations of the Earth's surface including all natural and built features, can be created many ways, including directly through lidar acquisitions or indirectly through photogrammetric manipulation of aerial imagery. DSMs created using aerial imagery collected via unmanned aircraft systems are prone to having high elevation error in places with vegetation, because the photographs capture only the top-most surface and do not penetrate to the underlying topography. While many studies have acknowledged this error, few have quantified its magnitude and extent especially for areas involving wild grasses or areas of drastic elevation change. While a distinct correlation between grass height and DSM vertical accuracy was not found, this study assesses possible reasons for model inaccuracy and possible future improvement.

TABLE OF CONTENTS

Chapter Page

LIST OF TABLES

Table Page

LIST OF FIGURES

Figure Page

# I. INTRODUCTION

## 1.1. BACKGROUND

The development of more affordable technology has expanded the horizons of what can be done with unmanned aircraft systems (UAS), allowing researchers to collect high resolution aerial images of individual study areas. Using Structure from Motion (SfM), a photogrammetric processing technique that matches objects from areas of overlap within aerial images to create accurate, three-dimensional (3D) models, researchers have been creating digital surface models (DSM). This UAS-SfM approach has been used to study a wide variety of applications, including archaeology (Jorayev et al., 2016), geomorphology (Lomolino et al., 2010), environmental monitoring (Turner et al., 2015; Ruzic, 2014), and agricultural modeling (Possoch et al., 2016). In some cases, the vertical accuracy of the DSMs created using the SfM method have been found to be comparable to light detection and ranging (lidar) data collected from a piloted aircraft (Bi et al., 2017; Fonstad et al., 2013), but UAS are able to be deployed more rapidly than manned aircraft, are relatively inexpensive to acquire, and are capable of low altitude data collection (Rango et al., 2009).

Gathering aerial photos and generating topographic data using the UAS-SfM methodology is frequently employed in barren landscapes such as glaciers, cliffs, and landslides, as well as for building structure, but fewer studies have focused on the

topography of vegetated areas. Vegetation itself has been listed in many studies as a known source of error, but few studies have quantified the magnitude and extent of this error. This study seeks to contribute to current research by quantifying how much vertical error different types of grass communities contribute to UAS-SfM-derived models and investigating if this error is reliable enough to be used to predict ground measurements. In this work, the term vertical error or height uncertainty refers to the discrepancy between actual ground elevation and elevation estimated by SfM. The following literature review provides a conceptual foundation and framework for this thesis.

### 1.1.2 UNMANNED AIRCRAFT SYSTEMS AND STRUCTURE FROM MOTION

Photogrammetry has traditionally relied on images collected from piloted aircraft, with stereo pairs of photos allowing the direct measurement of elevation and feature heights. With increasing availability and development of technology, both the image collection and photogrammetric techniques have been automated, and high resolution 3D datasets are now being created with ease across the geosciences (Fonstad et al., 2013).

SfM was initially developed to survey individual buildings or small objects (Snavely et al., 2008), although many studies have begun to use it to create 3D topographic datasets (Fonstad et al., 2013). SfM works by identifying corresponding features in different photographs using the Scale Invariant Feature Transform (SIFT) algorithm (Lowe, 2004), which uses computer vision techniques to detect and match local features in images. The Bundler tool then takes these matched features and adjusts them to identify their 3D position, orientation of the cameras, and the x,y,z location for each point located (Snavely et al., 2008). This information is used to create a sparse 3D point

cloud of features identified in the input photographs (Lucieer et al., 2014). A dense point cloud is then created using multi-view stereo (MVS) photogrammetry (e.g., PMVS [Furukawa and Ponce, 2009], CMVS [Furukawa et al., 2010])—i.e. SfM-MVS, simply referred to as SfM (Carrivick et al., 2016). The final model is often exported as a DSM raster, but this format simplifies points to fit a grid system and can be a source of error. Deriving accuracy by using point-to-point comparisons is more representative of true error (Wiseman et al., 2015).

All matched points are plotted in 3D space (i.e. x,y,z coordiantes). These thousands to millions of points are referred to in their entirety as a point cloud (like lidar data). Digital Terrain Models (DTMs) represent the elevation of bare earth across a landscape, while DSMs model the elevation of the entire landscape, including objects such as buildings and trees. Because SfM products such as DTMs and DSMs are derived from photos, there is only a single height value (z) associated at each x,y location, which is in contrast to products such as lidar-derived DTMs where there can be multiple height returns for each location. Therefore, SfM-derived products will frequently measure the top of vegetation as if it were ground, and accuracy may be compromised. Despite the importance of knowing the exact amount of error due to different vegetation types in SfM-derived products, a thorough understanding of vegetation effects is lacking.

The creation of a topographic model with the aerial photogrammetric method begins with the flight of a camera. There are multiple forms of aerial devices used to acquire imagery, including kites and helium blimps (Fonstad et al., 2013), but UAS are increasingly being used by researchers who cite the benefits of automated flight (Carbonneau and Dietrich, 2017). UAS can be programed to fly predetermined flight

paths over the study area capturing images with a mounted camera. The objective of these flights is to capture as much of the study area as possible, from many different angles. Photos taken from nadir, the angle directly above the study area, are the most common, but this orientation only captures the results in more occlusion and detail can be missed (Harwin and Lucieer, 2012). To get a more detailed and accurate model, researchers have found that including multiple passes flown from angles oblique to the study area increases the accuracy of the end model (Lucieer et al., 2014). Accuracy can also be increased by creating sufficient overlap of photographs, typically 70-80% forward and 60-70% sidelap (Singh and Frazier, 2018; Lucieer et al., 2014).

### 1.1.3 ACCURACY

Accuracy assessment is the best way to examine the quality of the topographic model (Bi et al., 2017). Unlike with traditional photogrammetry, SfM algorithms generate point locations arbitrarily, i.e. without the added use of ground control points (GCPs) to create a 3D model (Snavely et al., 2008). However, georeferencing the model using GCPs increases the overall model accuracy (Turner et al., 2012; Aguera-Vega et al., 2016). There are two common methodologies for georeferencing. The first method uses the UAS onboard Global Navigation Satellite System (GNSS) receiver to geotag the coordinates for each image taken (Singh and Frazier, 2017). These location data are then used to assist in camera identification for model creation and for georeferencing the model to a real-world coordinate system. Using coordinates from the UAS is referred to as the ‘direct’ method, but due to the instability of the aircraft and quality of the onboard GNSS receiver, these measurements can be less accurate than desired especially for high detail studies (Turner et al., 2012). A more accurate method is the ‘indirect’ method (Bi

et al., 2017), where the coordinate system is georeferenced using GCPs. These point locations are measured *in situ* with a high accuracy GPS, and the coordinates are used during processing to reference the model to a real-world coordinate system and to increase accuracy. After processing, the model's accuracy is measured using check points (CP). These are flat, usually bare ground points measured across the landscape, but unlike GCPS, CPs are not used in model creation. Bi et al. (2017) demonstrated that that use of GCPs can significantly increase the overall accuracy of the model. In this case, the direct method yielded an average error of 2-3m, while the indirect method yielded an average error of 0.4m. Carbonneau and Dietrich (2017) suggest the direct method is comparable to the indirect but that more research is needed on this front.

Accuracy protocols, as provided by Federal Geographic Data Committee (FGDC) and the American Society for Photogrammetry and Remote Sensing (ASPRS), include having at least 20, but recommended 30, spatially distributed GCPs that are measured with at least three times more accuracy than the derived dataset. Accuracy protocols also recommend that tests be reported with a 95% confidence interval, and values should be tested for normality and skewness. If the error is normally distributed, vertical accuracy should be reported as 1.9600* vertical RMSE (Federal Geographic Data Committee, 1998; Wiseman et al., 2015). Many individual studies agree that there is a threshold number of GCPs above which root mean square error (RMSE) does not increase (Singh and Frazier, 2017). For example, Aguera-Vega et al. (2016) suggest around 15 - 20 GCPs per $km^2$, while Gindraux et al. (2017) suggest a wider range of 10 - 20 GCPs. Both studies were executed in areas with little to no vegetation or terrain change.

## 1.2. TERRAIN MAPPING

DTMs represent the height of the bare earth surface and are valuable tools for analysis. As such, they are used in a variety of disciplines including hydrological and erosion modeling (Wiseman et al., 2015). In multiple instances, SfM has been used to accurately create point clouds and DTMs of barren areas that are comparable in accuracy to lidar. Fonstad et al. (2013) mapped a stone riverbed with a handheld helium blimp. To calculate accuracy, the resulting SfM point cloud was compared to airborne lidar using point-to-point comparison (Carrivick et al., 2016). The average distance between SfM and lidar points was 27 cm, but the average distance just for the z direction was 60 cm. This study considered these results to be closer in accuracy to terrestrial laser scanning (TLS) but comparable to aerial lidar. A similar but more accurate method was put forth by Long et al. (2016), who created a DSM of tidal dunes in a lagoon inlet system. Accuracy was derived from CPs, and the authors found a 17 cm difference between the two datasets.

The UAS-SfM method has been used to study a variety of different landforms, but most studies have focused on areas barren of vegetation (e.g., glaciers, sand dunes, river beds). Many of these studies have examined landslides to estimate soil movement. For instance, Niethammer et al. (2012), when studying a landslide with UAS photogrammetry, was able to create a model with a horizontal mean error of 5m. High error was attributed to the methods used when ortho-mosaicking photos using ArcMap. This error was avoided in the Turner et al. (2015) landslide study. Using SfM to create the point cloud directly from images, the authors found an accuracy of 4-5 cm in the horizontal and 3-4 cm in the vertical, which is comparable to airborne lidar. Accuracy

was derived from the non-active areas of the landslide. Similarly, Ruzic et al. (2014) found that SfM photogrammetry can define complex geomorphic structures, in this case cliff and undercuts. This study calculated an accuracy of 7 cm, which is within the limits of real-time kinematic (RTK) GPS precision (Ruzic et al., 2014). Another study completed in an area with similar structure to the study area assessed in this Thesis was by Uysal et al. (2015). UAS photogrammetry was performed using Agisoft PhotoScan to create DEM of small, rocky landform. Accuracy was calculated by comparing the point cloud against RTK mapped CPs, finding a vertical accuracy of 6.62 cm. The sources of error addressed were: weather, vibrations, lens distortions, and software limitations. While the UAS photogrammetric method is not free of errors even without vegetation, the amount of error in DSMs caused by the presence of vegetation has yet to be studied.

### 1.2.1. VEGETATION MAPPING

Due to photogrammetry being image-based, SfM data models are limited by visual line of sight. The creation of accurate DTMs can be difficult in areas where vegetation covers the ground, because SfM cannot penetrate vegetation to map the ground beneath as lidar can. While many studies have acknowledged vegetation sensing as a limitation of aerial photogrammetry (Bi et al., 2017; Johnson et al., 2014; Tonkin et al., 2014; Jorayev et al., 2016), few have assessed the impact of vegetation on DSM accuracy, specifically grasses.

Even sparse vegetation can cause errors (Jorayev et al., 2016). Bi et al. (2017) and Johnson et al. (2014) listed object-based image analysis (OBIA) as a method of identifying vegetation for possible removal from the model. Rango et al. (2009)

quantified grasses in UAS imagery using OBIA, but this method only measures location and amount of land cover, not elevation beneath the vegetation, vegetation height, or plant density. Once identified, areas representing vegetation in the model can be removed, but this process isn't necessarily practical. Jorayev et al. (2016) applied this method to a model of an archeological site but had to include some vegetation points in the final model to reduce the chance of smoothing actual topographic features. Even in areas where all vegetation points can be removed, the ground elevation values underneath the vegetation must be created based on an interpolation of the surrounding bare earth (Gillan et al., 2014) and are not necessarily accurate.

Vegetation height and density are good indicators of habitat quality for many types of wildlife, and many photogrammetric studies have been applied to measuring flora without measuring the underlying topography. SfM-UAS has been successfully used to measure the leaf area index (LAI) in vineyards (Mathews and Jensen, 2013). This ratio of leaf surface area to ground surface area describes canopy density (Johnson, 2003), which can be used to estimate vegetation vitality, and biomass (Mathews and Jensen, 2013).

Estimation of shrub height and crown size in a rangeland area using SfM is also a proven possibility. In a DSM created from UAV imagery, Gillan et al. (2014) identified shrubs with OBIA, removed these points from the data by hand, and then interpolated new bare ground points into the holes to create a DTM. Vegetation height was then measured by subtracting the DSM from the DTM to create a normalized DSM or nDSM with relative heights from ground-level. On the ground, shrub location, height, species, and amount of ground cover were measured in field plots. A Pearson's correlation

analysis between the photogrammetric and *in situ* measurements yielded significantly low mean height estimates from SfM for all shrubs, as SfM underestimated the shrub heights. However, dense shrubs were easier to discern from the landscape and were frequently measured more accurately. Grasses were too short to be adequately measured (Gillan et al., 2014).

#### 1.2.1.1. APPLICATIONS IN GRASS DOMINATED VEGETATION

Applying aerial photogrammetric approaches to estimating heights of small vegetation had not been common because of the high resolution data needed for accuracy. This limitation has been somewhat resolved with the development of affordable higher resolution cameras (Gillan et al., 2014). The technology has been commonly applied to studies on agricultural vegetation, but not many have focused on solely grasses and other vegetation types that are not planted in systematic patterns (i.e. agriculture; Possoch et al., 2016).

Tonkin et al. (2014) measured vegetation error as a side study while mapping the topography of a landscape using SfM. They compared the RMSE of shrubs to the RMSE of combined grasses and bare ground. The final model was compared to a 7,000-point total station survey to calculate RMSE. Unlike Gillan et al. (2014), this study did not compare the RMSE values to ground measurements of vegetation. Both studies agreed that photogrammetric methods are more accurate in areas with dense vegetation compared to sparse vegetation. Tonkin et al. (2014) found that dense vegetation produces a higher RMSE value compared with areas of sparse vegetation, up to 0.434 m in some

areas. Specific grass height and density was not mentioned, but as they were grouped with areas of bedrock, it can be assumed they were shorter than the shrubs.

Possoch et al. (2016) measured grass height in an agricultural setting using SfM and UAS. Fitting with previous studies, they discovered that short grasses were frequently underestimated, and tall grasses were overestimated. This study determined that plant height as estimated by UAS is a reliable indicator of biomass, but further research is needed for validation (Possoch et al., 2016). While this study addresses the ability for UASs to measure biomass and distinguish different grass heights when compared to a separate DTM, it does not address the impact of grass on DSM vertical accuracy.

## 1.3. A CALL FOR FURTHER RESEARCH

A rigorous assessment of the impact of grasses on vertical accuracy of DSMs derived from UAS-SfM in areas with ample topographic relief is missing to date. This study contributes to these initiatives by comparing elevation measurements based on UAS collected SfM photogrammetry to various heights and densities of grasses to assess if there is a predictable pattern between RMSE and grass height and density. This study will answer the following questions:

(1) Does grass height impact SfM-derived DSM accuracy?

(2) Does grass density impact SfM-derived DSM accuracy?

(3) Is there a predictable relationship between the accuracy of the DSM as measured by root mean square error (RMSE) and grass height/density?

# II. DATA AND METHODS

## 2.1 STUDY SITE

This study focused on the largest mesa at Gloss Mountain State Park located near Fairview, Oklahoma (36.3620836 W, -98.582022 N) (Figure 1). Gloss Mountain, typically pronounced ‘glass’, is named for the sparkling selenite crystals that top the mountain and are eroding down the sides. The landscape is a series of mesas and buttes remaining from the retreating Blaine Escarpment, with the highest point in the park standing about 60 m above the surrounding plains, 490 ft above sea level (McPhail and Marston, ND.). Abrupt changes in elevation make this area a great candidate to study error within UAS photogrammetry models, as most accuracy studies have been carried out on relatively flat areas, and findings may not be generalizable to areas with different elevation types (Singh and Frazier, 2018). The park itself is almost one square mile and contains three main topographic features, but this study focuses only on the main mesa in the middle and the immediate surrounding land (Figure 1). A gravel road winds around the north side of the mesa to numerous oil well pads, providing flat bare ground for quality checkpoints. Vegetation typical of the mixed grass prairie covers much of the sides and base of the mesa including big bluestem (*Andropogon gerardii*), little bluestem

(*Schizachyrium scoparium*), Cattail (*Typha angustifolia*), Saltgrass (*Distichlis spicata*), silver stem grasses (*Botriochloa* spp.), *Chenopodiaceae* and other forbs, accompanied by scattered Juniperous virginia (Figure 2).

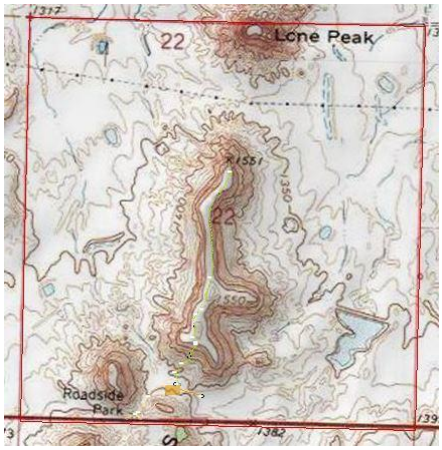


Figure 1. Gloss Mountain State Park with USA Topo Map basemap.

Figure 2: Oblique photo of the northernmost point of the mountain covered by grasses and juniper.

## 2.2 UAS SURVEYS

Data for all steps of this research were gathered with permission from the Oklahoma State Parks. Aerial imagery was collected within two hours of solar noon on a sunny day with minimal clouds in November 2017. Two automated flights were performed using a DJI Phantom 4 Pro with the standard camera attachment: 1/2.3" CMOS camera sensor with 12.4 M effective pixels. The aircraft was flown 122 m above the ground along parallel, approximately east-west flight paths with 80/60% forward/side overlap. The first flight path captured the entire mountain from a nadir perspective (Figure 3), and the second flight captured half the mountain with obliques at a 45° angle from the ground (Figure 4). Both flights were completed in several segments to permit battery changes whereby the UAS landed, the battery was changed, and the platform

automatically resumed its flight where it had left off. In total, the flights captured 1,427 photos with a 3.8 cm resolution, which is high enough to differentiate species (Lu and He, 2017).

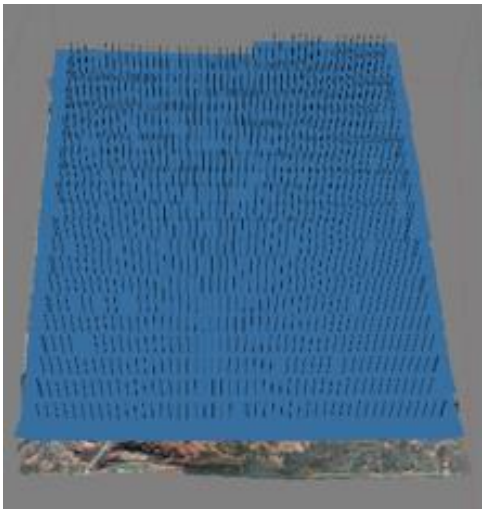

Figure 3: UAS-collected nadir-facing images

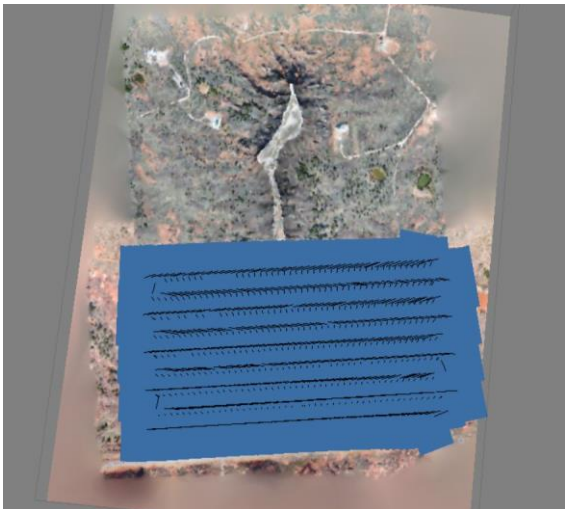

Figure 4: Oblique images captured for the southern half of the study area.

## 2.3 FIELD DATA

Prior to image acquisition, 31 GCPs were placed across the landscape, marked with paper plate targets (0.25 m diameter) (Figure 6) staked into the ground, with a black duct tape ‘X’ marking the center. Locations were randomly generated across the study site using the random point placement tool in ArcGIS, and the GCPs were placed as close to their assigned location as physically possible, given the terrain limitations. The GCPs were then mapped with a RTK GNSS unit (Figure 6) with a reported accuracy of 2 cm.

The corresponding base station tripod for the RTK unit was placed on top on the mountain in the southwest corner overlooking much of the study area (Figure 7).

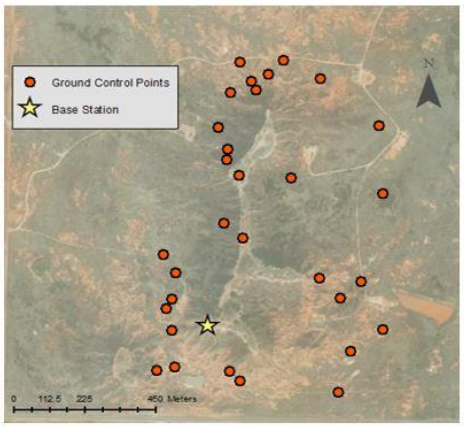


Figure 6: Ground Control Points (GCPs) spread across the landscape to measure a variety of elevations

Figure 5: Example paper plate GCP

Figure 7: The RTK base station on top of the mesa.

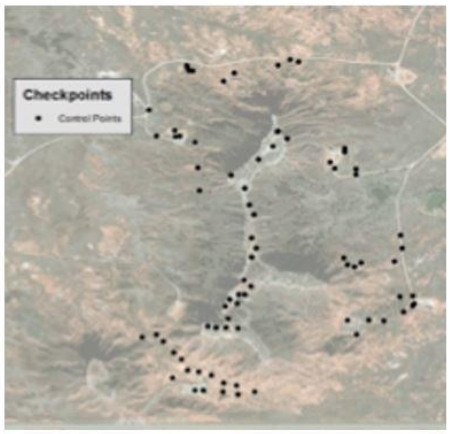


Figure 8: The checkpoints, including bare ground and grass plots, spread over the landscape.

Due to the sensitivity of collecting data within a State Park, permissions were granted in January 2018 to collect grass height and density measurements across the study area. The time lag between the flights in late November and these measurements in early January is not expected to impact results as the grasses were still dormant during the period (Figure 9). During the January data collection event, 30 2-$m^2$ grass plots were chosen to represent a variety of elevations and vegetation heights across the study area, with 10 points on top of the mountain and 20 around the edges and base (Figure 8). At each plot, five measurements of minimum and maximum grass heights were recorded, one at each corner and one in the center (Figure 9), using the direct method as described by Stewart et al. (2001). Photos and notes were taken to record species and a visual approximation of vegetation structure. To measure ground cover, average leaf area index

(LAI) readings were taken with an AccuPAR LP-80 (Decagon Devices) across each plot from the North/South, and East/West orientations. Each plot center was located with the RTK unit. Twenty CPs were collected with the RTK unit on areas of bare ground near the grass plots.

Figure 9: LAI readings were taken with an AccuPAR LP-80 (Decagon Devices) across each plot from the N/S, and E/W orientations (left). Tallest plot: 114in cattail species in a dry pond (right)

## 2.4 MODEL CREATION

Prior to image processing, all coordinate data were manually removed from the photos to ensure an indirect georeferencing unbiased from the UAS metadata. The clean aerial images were then processed using SfM in Agisoft PhotoScan.

A basic model was created using built-in processes within PhotoScan. First, images were aligned based on matching features between images. Because the photos had no location data, PhotoScan automatically calculated camera orientations and positions based on the images. From the aligned photos, a dense point cloud was generated on highest possible quality. Depth information was calculated based on the estimated camera positions (Agisoft, 2016). Once the process completed, noise and obvious outliers were manually removed from the point cloud.

The model was then georeferenced with the GCPs identified in each photo and tagged with their corresponding RTK-GPS coordinates. Before georeferencing, all RTK points were converted to a vertical orthometric with WGS 1984 projection using NOAA's Vdatum tool to increase accuracy. A first draft model included all 31 GCPs, but a heat map of error values discovered a GCP with coordinates measuring over 3 m from its marker. It was determined that this GCP was erroneous, and removal of this outlier improved local model accuracy. The final georeferenced point cloud was created and exported to ArcMap as a point cloud and a DSM raster.

## 2.5 VERTICAL ERROR CALCULATION

To assess the model's overall accuracy, the RMSE of height values was calculated against the bare ground CPs. The lowest RMSE values came from the DSM rasters because larger resolution DSMs smooth out small features likely to cause error (Gindraux et al., 2017). Although an unaggregated point cloud is the most accurate representation of a landscape (Wiseman et al., 2015), the 2 m DSM was chosen to match the relative accuracy of the averaged data from the 2 m grass plots. Computationally, processing the dense point cloud using ArcMap was intensive, making it difficult to create a 2 m plot with the grass point as the center, so the DSM was generated in SfM without reference to grass plot locations.

Point layers and DEMs were all projected to NAD1983 UTM Oklahoma North 2011 (m) in Arcmap. Height values were paired using the Extract Values to Points tool, and the resulting layer was exported to Excel for calculation.

## 2.6 GRASS ERROR CALCULATION

A variety of linear least squares regressions were calculated using Statistical Package for the Social Sciences (SPSS) software to assess possible causes of error and determine any relationship between variables. Independent variables included max grass height, average grass height, grass density as represented by mean LAI collected by the ceptometer, and grass species. The dependent variable was model error. Four variables presented skewness in a normality check. Maximum grass height and average grass height were transformed logarithmically, and LAI and plot error with transformed with square root.

# III. RESULTS AND DISCUSSION

Multiple models were created in effort to test the most accurate SfM methodology for this data set, and the most successful model yielded an RMSE of 2.29 m. While the accuracy of this model is lacking, the final point cloud is evenly made, colorful, devoid of holes, and all around visually stunning (Figure 10). The method that improved this

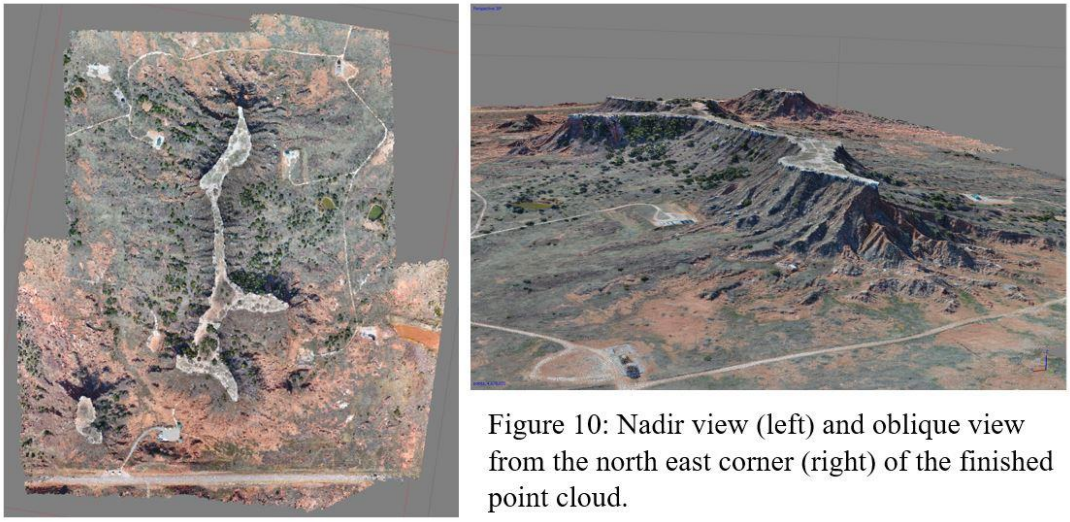

Figure 10: Nadir view (left) and oblique view from the north east corner (right) of the finished point cloud.

model above the others was increasing the "quality" setting during dense cloud creation. SfM sets the default setting to "lowest" to reduce processing time, but increasing the quality obtains more detailed and accurate geometry because the processing is done with original photos, instead of downsizing them to save time (Agisoft PhotoScan User

Manual, 2016). Despite differences in computational efficiency (this highest accuracy model required 8.5 days longer to process), the vertical RMSE results are relatively similar to the low setting: 2.49 m vs. 2.29 m, for the lowest and highest respectively.

Overall, model vertical error measured by the control points ranges from -0.96 to 5.43, and the grass plot error ranges from -1.2 to 4.7. While there is variation among the grass plot error, it seems to be more related to spatial location than to any of the grass variables. The tallest grass plot was dominated by a cattail species (44.88 cm) located on the northwest side of the mesa with a vertical error of 2.92 m. The shortest grass plot (1.65 cm) also on the northwest side of the mountain has a similar error of 2.13 m. The full table of these grass values can be found in Appendix A, and Table 1 shows species averages and standard deviations. If grass height was the main cause of error in this model, we would expect these tallest and shortest grass measurements to mirror the range of the overall error, instead of their location as they do now. Measuring grass height through height uncertainty requires that there be minimal uncertainty from other factors, and that does not appear to be the case in this model.

| Dominant Species | Big Bluestem | Little Bluestem | Beardgrass | Forbs | Cattail | Saltgrass |
|---|---|---|---|---|---|---|
| # of Plots | 4 | 5 | 14 | 3 | 1 | 3 |
| Avg. Vertical error (m) | 2.00 | 1.78 | 0.84 | 2.91 | 2.92 | 1.88 |
| St.Dev. | 0.84 | 2.20 | 0.69 | 1.37 | | 1.93 |
| Average LAI | 2.95 | 2.32 | 2.38 | 1.16 | 1.8 | 1.48 |
| St.Dev. | 0.69 | 0.99 | 1.61 | 0.38 | | 0.81 |
| Avg. Grass Height | 8.19 | 13.01 | 10.23 | 9.29 | 21.26 | 3.66 |
| St.Dev. | 2.23 | 4.97 | 3.32 | 1.46 | | 1.44 |

Table 1: Plot averages by dominant species.

Regression results found neither correlation nor significance in prediction capability for any of the variables tested. Forward and backward stepwise regressions were performed, but no variables were found to be significant enough to be included. Error regressions were performed with a variety of different data combinations, without species data, abnormally distributed variables were transformed, yet no significant results arose (Table 2). While it is reasonable to assume based on previous research that some of the model error was caused by grasses (Possoch et al., 2016), there appears to be too much error from other sources (see Section 3.1) to draw any firm conclusions from these data. The following section will assess other possible sources of error based on the spatial distribution.

**Model Summary[b]**

| Model | R | R Square | Adjusted R Square | Std. Error of the Estimate |
|---|---|---|---|---|
| 1 | .602[a] | .363 | .061 | 1.747820518 |

a. Predictors: (Constant), Saltgrass, Cattail, Cheno, Forb, Big Bluestem, Little Bluestem, LAI, AvgGrass, MaxGrass

b. Dependent Variable: Error(m)

Table 2: Results of the enter regression with all original variables

## 3.1. OVERALL MODEL ERROR

RMSE of the GCPs was 1.12 m. as calculated by SfM. Adjusting the GCP pins to match the computer suggested points (as marked by blue flags) did decrease RMSE to almost 0, but the flags were often several meters away from the paper plate markers. While it's unclear exactly how this is calculated, it might indicate that at least part of the model's overall vertical error must originate in the construction of the point cloud and is not necessarily introduced by just grasses.

The overall model has issues common in studies concerning topography and vegetation. To decrease the chance of grass pixels getting filtered out as noise, when creating the dense cloud, the depth filtering option was changed from the SfM default *aggressive,* to *moderate*. This step created a very noisy and inaccurate point cloud, so it is thought this setting is possibly designed to be effective with higher resolution imagery. In a future study, decreasing the flying height could increase resolution and therefore increase overall model accuracy (Santise et al., 2014), but it would also increase the time required for image capture along with the number of photos and time needed for processing. Time is important especially when working with a study area of this size, because the passing of the sun increases the change in shadows between nadir and oblique photo collections. Shadows are an issue because they introduce a change in visual pattern on the landscape that can be interpreted by SfM as an individual surface. While none of the grass plots lay in the shadow of the mesa itself and collecting near solar noon minimized the length of shadows, there are still shadows within the grasses that could have caused misreadings with SfM (Figure 11). In another study by Mortensson et al. (2017), the appearance of shadows in 4 cm grass on flat ground increased height

uncertainty (RMSE) in a DEM produced with Agisoft PhotoScan by a factor of four. The authors suggested that flying under total cloud cover could further minimize shadows, although this could decrease reflectance and contrast, leading to a less accurate DSM.

Error also could have been caused by the difference in color between nadir and oblique photos. Oblique photos captured the region's bright red soil more vibrantly than the nadir (Figure 11), which could have been difficult for the feature-matching algorithm in SfM to interpret. If this were the dominant cause of error, there would be a north/south spatial pattern in the distribution of error matching the half of the mesa covered by the oblique photos, instead of the existing east/west distribution. Even though it is not the dominant cause of error, this still may have introduced some error when measuring depth.

Figure 11: Difference in color between the oblique (left) and nadir (right) images

The output from SfM with the least amount of vertical error is the 2 m resolution DSM. Although point clouds are known to be more accurate (Wiseman et al., 2015), there were technical issues with managing such a large file across software platforms. Exporting the full point cloud provided too much data for ArcMap to process, yet only exporting the areas of concern caused an error with the .laz to .las convertor, assumedly due to the lack of spatial continuity of that

data. The optimal situation would create each cell in the DSM to overlap centroids with the grass plots. It is unclear exactly how SfM calculates DSM rasters, but as it is unlikely that each cell perfectly overlaps the grass plots, this inclusion of points bordering the grass plots is worth considering as a source of error.

Figure 11. An example nadir photo captured along the edge of the mesa showing small shadows within the grasses.

## 3.2 SPATIAL DISTRIBUTION OF MODEL ERROR

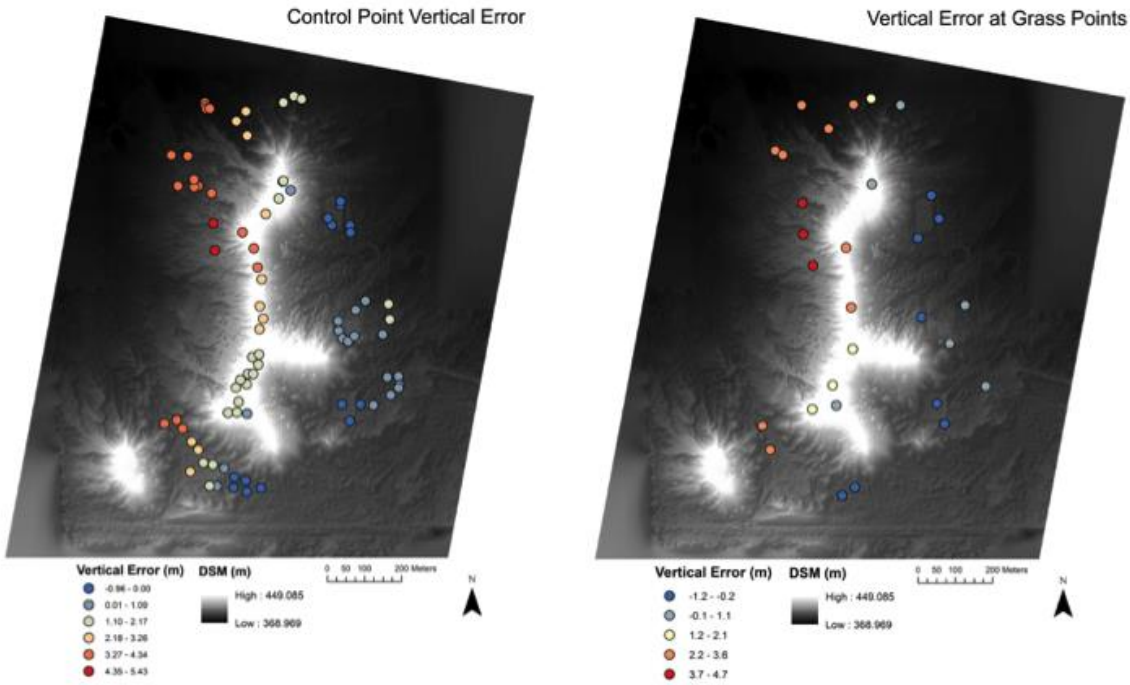


Figure 12: Error distribution in the model has an east/west pattern.

The most distinct result for all of the models created with this dataset is the spatial distribution of vertical height error across the mesa. The point cloud shows a general pattern of west to east decrease in error (Figure 12). This model has a distinct east/west pattern to the errors, where points on the west side of the mesa are generally overestimated, while the points on the east are underestimated (Figure 12). This error distribution was not likely caused by the flightlines, as those ran east and west. The pattern also doesn't follow the route the RTK took when measuring plot points. Error distributions also appear to be spatially independent of average LAI and average grass height per plot. Although there are

many more plots dominated by *Botriochloa* species on the east side, the error underestimation pattern isn't limited to those plots, indicating that this error is also independent of dominant grass type. Maps of these three variables can be found in Appendix B. An additional regression was attempted for this model with the addition of elevation values, but results did not change. There does not appear to be any large shadows in the model, except for around the immediate edges of the mesa away from any check or grass points. During collection, the sun angle was primarily from the south, and rose to the south west during image capture (starting altitude of 32.5, Azimuth E of N was 167.5 (Astronomical Applications Dept., 2018). There is a chance that this error pattern was caused by a camera angle issue, difference in shadows, or a change in lens glare, which has been known to cause error in models (Uysal, 2015).

## 3.3 CONCLUSION

This project created a DSM using UAS collected aerial imagery of Gloss Mountain State Park to measure the impacts of grass height and significant topography on DSM accuracy. Average grass height for the study area was 0.79m, which was stifled by the extra error from the rest of the model's RMSE of 2.29 m. There are many probable factors that led to the model's high RMSE value including a difference in color between nadir and oblique images and possible lens glare from the sun. Regressions attempting to predict grass height, density, and species found neither correlation nor significance. In sum, there appears to be too much noise from the additional model error to determine exactly how much error originated from the grasses. Other studies have been successful at creating models with Agisoft PhotoScan SfM of topography (Ruzic et al., 2014), of

vegetation (Possoch et al., 2016), and identifying species (Lu and He, 2017), therefore in the future with more accurate data, it is reasonable to assume species identification in areas with topography using UAS derived data can be completed.

# REFERENCES


Agisoft, 2016. Agisoft PhotoScan user manual: professional edition Version 1.2. Retrieved 5/2018. http://www.agisoft.com/pdf/photoscan-pro_1_2_en.pdf

Agüera-Vega, F., Carvajal-Ramírez, F. and Martínez-Carricondo, P., 2017. Assessment of photogrammetric mapping accuracy based on variation ground checkpoints number using unmanned aerial vehicle. *Measurement*, 98, pp.221-227.

Astronomical Applications Dept. - U.S. Naval Observatory. Sun or Moon Altitude/ Azimuth Table, Fairfiew Ok, Jan 19 2018. Accessed November 2018. http://aa.usno.navy.mil/data/docs/AltAz.php

Bi, H., Zheng, W., Ren, Z., Zeng, J. and Yu, J., 2017. Using an unmanned aerial vehicle for topography mapping of the fault zone based on structure from motion photogrammetry. *International Journal of Remote Sensing*, 38(8-10), pp.2495-2510.

Carbonneau, P.E. and Dietrich, J.T., 2017. Cost-effective non-metric photogrammetry from consumer grade sUAS: implications for direct georeferencing of structure from motion photogrammetry. *Earth Surface Processes and Landforms*, *42*(3), pp.473-486.

Carrivick, J., M. Smith, and D. Quincey., 2016. *Structure from motion in the geosciences*. Wiley-Blackwell.

Federal Geographic Data Committee, 1998. Geospatial Positioning Accuracy Standards, part 3: National standard for spatial data accuracy. *Subcommittee for Base Cartographic Data, 25p*.

Fonstad, M.A., Dietrich, J.T., Courville, B.C., Jensen, J.L. and Carbonneau, P.E., 2013. Topographic structure from motion: a new development in photogrammetric measurement. *Earth Surface Processes and Landforms*, *38*(4), pp.421-430.

Furukawa, Y. and Ponce, J., 2009. Carved visual hulls for image-based modelling. International Journal of Computer Vision, 81, 53–67.

Furukawa, Y., Curless, B., Seitz, S.M. & Szeliski, R., 2010. Towards internet-scale Multi-View Stereo. In: IEEE Conference, Computer Vision and Pattern Recognition (CVPR), June 13–18, 2010, pp. 1434-1441. San Francisco, CA.

Gillan, J.K., Karl, J.W., Duniway, M. and Elaksher, A., 2014. Modeling vegetation heights from high resolution stereo aerial photography: An application for broad-scale rangeland monitoring. Journal of environmental management, 144, pp.226-235.

Gindraux, S., Boesch, R. and Farinotti, D., 2017. Accuracy assessment of digital surface models from unmanned aerial vehicles' imagery on glaciers. *Remote Sensing*, *9*(2), p.186.

Harwin, S. and Lucieer, A., 2012. Assessing the accuracy of georeferenced point clouds produced via multi-view stereopsis from unmanned aerial vehicle (UAS) imagery. Remote Sensing, 4(6), pp.1573-1599.

Johnson, L.F., 2003.Temporal stability of an NDVI-LAI relationship in a Napa Valley vineyard. Aust. J. Grape Wine Res. 9, 96–101.

Johnson, K., E. Nissen, S. Saripalli, J. R. Arrowsmith, P. McGarey, K. Scharer, P. Williams, K. Blisniuk. 2014. Rapid mapping of ultrafine fault zone topography with structure from motion. Geosphere 10 (5): 969-86.

Jorayev, G., Wehr, K., Benito-Calvo, A., Njau, J. and de la Torre, I., 2016. Imaging and photogrammetry models of Olduvai Gorge (Tanzania) by Unmanned Aerial Vehicles: A high-resolution digital database for research and conservation of Early Stone Age sites. *Journal of Archaeological Science*, *75*, pp.40-56.

Lomolino, M.V., Riddle, B.R., Whittaker, R.J. and Brown, J.H., 2010. Biogeography (Sinauer, Sunderland, MA).

Long, N., Millescamps, B., Guillot, B., Pouget, F. and Bertin, X., 2016. Monitoring the topography of a dynamic tidal inlet using UAS imagery. *Remote Sensing*, *8*(5), p.387.

Lowe, D.G., 2004. Distinctive image features from scale-invariant keypoints. *International journal of computer vision*, *60*(2), pp.91-110.

Lu, B. and He, Y., 2017. Species classification using Unmanned Aerial Vehicle (UAV)-acquired high spatial resolution imagery in a heterogeneous grassland. ISPRS Journal of Photogrammetry and Remote Sensing, 128, pp.73-85.

Lucieer, A., Jong, S.M.D. and Turner, D., 2014. Mapping landslide displacements using Structure from Motion (SfM) and image correlation of multi-temporal UAS photography. Progress in Physical Geography, 38(1), pp.97-116.

Mårtensson, S.G. and Reshetyuk, Y., 2017. Height uncertainty in digital terrain modelling with unmanned aircraft systems. Survey review, 49(355), pp.312-318.

Mancini, F., Dubbini, M., Gattelli, M., Stecchi, F., Fabbri, S. and Gabbianelli, G., 2013. Using unmanned aerial vehicles (UAS) for high-resolution reconstruction of topography: The structure from motion approach on coastal environments. Remote Sensing, 5(12), pp.6880-6898.

Mathews, A.J. and Jensen, J.L., 2013. Visualizing and quantifying vineyard canopy LAI using an unmanned aerial vehicle (UAV) collected high density structure from motion point cloud. *Remote Sensing*, *5*(5), pp.2164-2183.

McPhail, M.L., and Marston R. A. ND. "Glass Mountains," *The Encyclopedia of Oklahoma History and Culture*, www.okhistory.org (accessed May 1, 2018).

Melanie L. McPhail and Richard A. Marston, "Glass Mountains," *The Encyclopedia of Oklahoma History and Culture*, www.okhistory.org (accessed May 1, 2018).

Niethammer, U., M. R. James, S. Rothmund, J. Travelletti, M. Joswig. 2012. UAS-based remote sensing of the Super-Sauze landslide: Evaluation and results. *Engineering Geology* 128: 2-11.

Possoch, M., Bieker, S., Hoffmeister, D., Bolten, A., Schellberg, J. and Bareth, G., 2016. Multi-temporal crop surface models combined with the RGB vegetation index from UAS-based images for forage monitoring in grassland. The International Archives of Photogrammetry, Remote Sensing and Spatial Information Sciences, 41, p.991.

Rango, A., Laliberte, A., Herrick, J.E., Winters, C., Havstad, K., Steele, C. and Browning, D., 2009. Unmanned aerial vehicle-based remote sensing for rangeland assessment, monitoring, and management. *Journal of Applied Remote Sensing*, *3*(1), p.033542.

Reshetyuk, Yuriy, and Stig-Göran Mårtensson. 2016. "Generation of highly accurate digital elevation models with unmanned aerial vehicles." The Photogrammetric Record 31, no. 154: 143-165.

Ružić, I., I. Marović, Č. Benac, and S. Ilić. 2014. Coastal cliff geometry derived from structure-from-motion photogrammetry at Stara Baska, Krk Island, Croatia. *Geo-Marine Letters* 34 (6): 555-65.

Santise, M., Fornari, M., Forlani, G. and Roncella, R., 2014. Evaluation of DEM generation accuracy from UAS imagery. International Archives of Photogrammetry, Remote Sensing and Spatial Information Sciences, 40(5): 529–536.

Singh, K.K. and Frazier, A.E., 2018. A meta-analysis and review of unmanned aircraft system (UAS) imagery for terrestrial applications. *International Journal of Remote Sensing*, pp.1-21.

Snavely, N., Seitz, S.M. and Szeliski, R., 2008. Modeling the world from internet photo collections. *International journal of computer vision*, *80*(2), pp.189-210.

Stewart, K.E.J., Bourn, N.A.D. and Thomas, J.A., 2001. An evaluation of three quick methods commonly used to assess sward height in ecology. Journal of Applied ecology, 38(5), pp.1148-1154.

Tonkin, T.N., Midgley, N.G., Graham, D.J. and Labadz, J.C., 2014. The potential of small unmanned aircraft systems and structure-from-motion for topographic surveys: A test of emerging integrated approaches at Cwm Idwal, North Wales. *Geomorphology*, *226*, pp.35-43.

Turner, D., Lucieer, A. and Watson, C., 2012. An automated technique for generating georectified mosaics from ultra-high resolution unmanned aerial vehicle (UAS) imagery, based on structure from motion (SfM) point clouds. *Remote sensing*, *4*(5), pp.1392-1410.

Turner, D., A. Lucieer, S. M. de Jong. 2015. Time series analysis of landslide dynamics using an unmanned aerial vehicle (UAS). *Remote Sensing* 7: 1736-57.

Uysal, M., A. S. Toprak, N. Polat. 2015. DEM generation with UAS photogrammetry and accuracy analysis in Sahitler hill. *Measurement* 73: 539-43.

Wiseman, D.J. and van der Sluijs, J., 2015. Alternative Methods for Developing and Assessing the Accuracy of UAS-Derived DEMs. *International Journal of Applied Geospatial Research (IJAGR)*, *6*(3), pp.58-77

# APPENDICES

*Appendix A. Grass plot results*

| Plot | Error(m) | AvgMaxGrass | AvgGrass | LAI | Dom.Species | Co-Dom.Species |
|---|---|---|---|---|---|---|
| 1 | 1.748139014 | 11.57 | 5.04 | 3.39 | Big Bluestem | Little Bluestem |
| 2 | 0.723674951 | 18.50 | 8.98 | 2.99 | Big Bluestem | |
| 3 | 1.645825879 | 7.17 | 1.73 | | Beardgrass sp | |
| 4 | 1.342040527 | 11.18 | 1.97 | 0.27 | Forb | Little Bluestem |
| 5 | 2.71799375 | 7.64 | 2.05 | 1.02 | Forb | Beardgrass sp |
| 6 | 2.787755176 | 13.94 | 7.56 | 3.59 | Big Bluestem | Little Bluestem |
| 7 | 1.051235986 | 10.55 | 3.39 | 0.87 | Little Bluestem | |
| 8 | 4.19681875 | 9.37 | 2.83 | 2.11 | Little Bluestem | |
| 9 | 4.570113428 | 22.60 | 12.76 | 3.45 | Little Bluestem | |
| 10 | 4.6763104 | 9.06 | 4.65 | 2.2 | Chenopodiaceae | Big Bluestem |
| 11 | 2.924664307 | 44.88 | 21.26 | 1.8 | Cattail | |
| 12 | 3.437651611 | 7.01 | 5.28 | 2.12 | Saltgrass | |
| 13 | 3.057850098 | 10.39 | 3.94 | 1.99 | Saltgrass | Little Bluestem |
| 14 | 3.092077051 | 12.20 | 5.67 | 4.13 | Beardgrass sp | Sideoats grama |
| 15 | 2.496416357 | 15.20 | 7.87 | 2.37 | Beardgrass sp | |
| 16 | 2.139457324 | 4.02 | 1.65 | 0.45 | Beardgrass sp | Saltgrass |
| 17 | 0.699309424 | 10.71 | 5.28 | 2.54 | Beardgrass sp | |
| 18 | -0.504390283 | 10.24 | 5.75 | 4.95 | Beardgrass sp | Little Bluestem |
| 19 | -0.53540332 | 9.61 | 4.80 | 1.401 | Beardgrass sp | Little Bluestem |
| 20 | -0.979993359 | 11.57 | 5.20 | 5.94 | Beardgrass sp | |
| 21 | 0.490702637 | 7.09 | 4.72 | 0.71 | Beardgrass sp | Little Bluestem |
| 22 | -0.204660059 | 12.99 | 7.40 | 3.4 | Little Bluestem | Botriochloa sp |
| 23 | 0.935110596 | 7.72 | 1.81 | 0.92 | Beardgrass sp | Big Bluestem |
| 24 | 0.40054707 | 12.05 | 5.43 | 1.89 | Beardgrass sp | Big Bluestem |
| 25 | -0.520347607 | 13.62 | 5.67 | 2.47 | Beardgrass sp | Big Bluestem |
| 26 | -0.692211426 | 9.53 | 3.70 | 1.76 | Little Bluestem | Switchgrass |
| 27 | 2.725210645 | 23.70 | 11.18 | 1.81 | Big Bluestem | |
| 28 | 3.642492187 | 15.67 | 5.35 | 1.42 | Beardgrass sp | Little Bluestem |
| 29 | -0.840986133 | 2.99 | 1.77 | 0.33 | Saltgrass | |
| 30 | -1.203753516 | 6.38 | 3.15 | 1.72 | Beardgrass sp | |

*Appendix B. Maps of dominant species, average grass height, and average LAI per plot:*

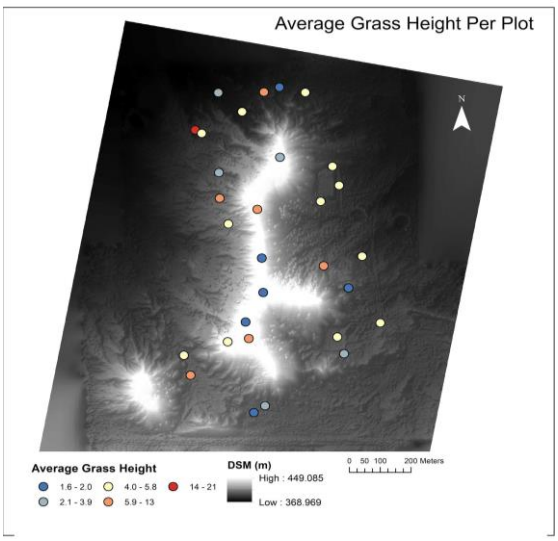


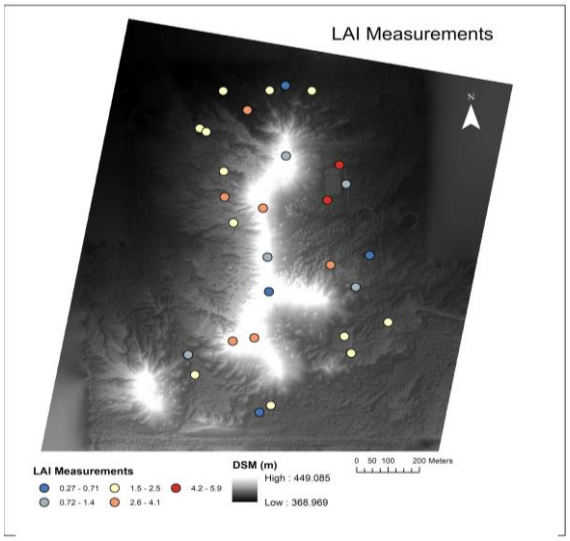


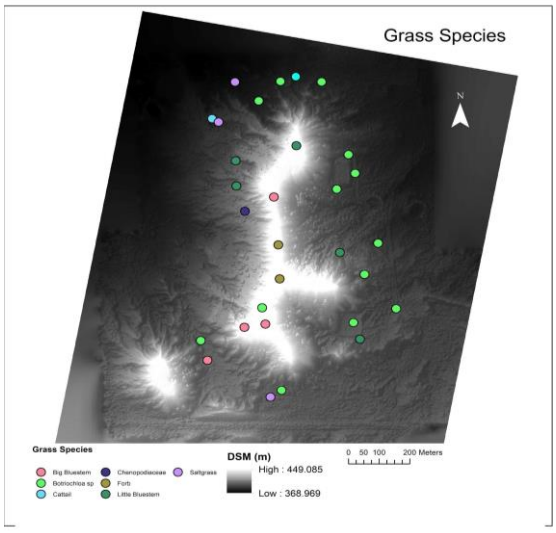

VITA

Amanda Fae Thomas

Candidate for the Degree of

Master of Science

Thesis: ASSESSING IMPACTS OF GRASS ON VERTICAL ACCURACY OF DIGITAL SURFACE MODELS DERIVED FROM UNMANNED AIRCRAFT SYSTEMS

Major Field: Geography

Biographical: Amanda Thomas is from Bartlesville, Ok.

Education:

Completed the requirements for the Master of Science in Geography at Oklahoma State University, Stillwater, Oklahoma in December, 2018.

Completed the requirements for the Bachelor of Science in Agriculture at Oklahoma State University, Stillwater, Oklahoma in December, 2016.

Experience: Graduate Research Assistant – Oklahoma State Parks mapping grant.

Professional Memberships:

Gamma Theta Upsilon - Geography honors society
Xi Sigma Pi - Forestry honors society
OSU Graduate and Professional Student Government Association